

Synergistic SERS effects in organic/MoS_2 heterojunctions with cavity structure enabling nanoplastics screening and antibiotic adsorption behavior detection

Liqi Ma(马立琪), Abdur Rahim(阿卜杜勒-拉希姆), Baiju Lü(吕白菊), Muhammad Saleem(穆罕默德-萨利姆), Xiaoyu Zhang(张晓雨), Mingyue Li(李明月), Muhammad Zahid(穆罕默德-扎希德), and Mei Liu(刘玫)
Citation: Chin. Phys. B, 2025, 34 (**4**): 047402. DOI: 10.1088/1674-1056/ada888
Journal homepage: http://cpb.iphy.ac.cn; http://iopscience.iop.org/cpb

What follows is a list of articles you may be interested in

SERS activity of carbon nanotubes modified by silver nanoparticles with different particle sizes

Xiao-Lei Zhang(张晓蕾), Jie Zhang(张洁), Yuan Luo(罗元), and Jia Ran(冉佳)
Chin. Phys. B, 2022, 31 (**7**): 077401. DOI: 10.1088/1674-1056/ac4f51

Low-energy (40 keV) proton irradiation of $YBa_2Cu_3O_{7-x}$ thin films:Micro-Raman characterization and electrical transport properties

San-Sheng Wang(王三胜), Fang Li(李方), Han Wu(吴晗), Yu Zhang(张玉), Suleman Mu?ammad(穆罕默德苏尔曼), Peng Zhao(赵鹏), Xiao-Yun Le(乐小云), Zhi-Song Xiao(肖志松), Li-Xiang Jiang(姜利祥), Xue-Dong Ou(欧学东), Xiao-Ping Ouyang(欧阳晓平)
Chin. Phys. B, 2019, 28 (**2**): 027401. DOI: 10.1088/1674-1056/28/2/027401

Ultrasensitive nanosensors based on localized surface plasmon resonances: From theory to applications

Wen Chen(陈文), Huatian Hu(胡华天), Wei Jiang(姜巍), Yuhao Xu(徐宇浩), Shunping Zhang(张顺平), Hongxing Xu(徐红星)
Chin. Phys. B, 2018, 27 (**10**): 107403. DOI: 10.1088/1674-1056/27/10/107403

Highly sensitive and stable SERS probes of alternately deposited Ag and Au layers on 3D SiO_2 nanogrids for detection of trace mercury ions

Yi Tian(田毅), Han-Fu Wang(王汉夫), Lan-Qin Yan(闫兰琴), Xian-Feng Zhang(张先锋), Attia Falak, Pei-Pei Chen(陈佩佩), Feng-Liang Dong(董凤良), Lian-Feng Sun(孙连峰), Wei-Guo Chu(褚卫国)
Chin. Phys. B, 2018, 27 (**7**): 077406. DOI: 10.1088/1674-1056/27/7/077406

The structure and elasticity of phase B silicates under high pressure by first principles simulation

Lei Liu(刘雷), Li Yi(易丽), Hong Liu(刘红), Ying Li(李营), Chun-Qiang Zhuang(庄春强), Long-Xing Yang(杨龙星), Gui-Ping Liu(刘桂平)
Chin. Phys. B, 2018, 27 (**4**): 047402. DOI: 10.1088/1674-1056/27/4/047402

Synergistic SERS effects in organic/MoS_2 heterojunctions with cavity structure enabling nanoplastics screening and antibiotic adsorption behavior detection

Liqi Ma(马立琪), Abdur Rahim(阿卜杜勒-拉希姆), Baiju Lü(吕白菊), Muhammad Saleem(穆罕默德-萨利姆), Xiaoyu Zhang(张晓雨), Mingyue Li(李明月), Muhammad Zahid(穆罕默德-扎希德), and Mei Liu(刘玫)†

School of Physics and Electronics, Shandong Normal University, Jinan 250358, *China*

(Received 8 January 2025; revised manuscript received 8 January 2025; accepted manuscript online 10 January 2025)

The detection of nanoplastics (NPs) and their interactions with antibiotics is critical due to their potential environmental and health risks. Traditional detection methods are challenged by the small size and chemical similarity of NPs to microplastics. Current surface-enhanced Raman scattering (SERS) substrates for NP detection are limited by high cost, reliance on single enhancement modes, and insufficient sensitivity and selectivity, especially for NP-antibiotic complexes. In this study, the F/M-AAO substrate, which integrates 2,3,5,6-tetrafluoro-tetracyanoquinodimethane (F_4TCNQ) and molybdenum disulfide (MoS_2) with anodic aluminum oxide (AAO) templates, is used to enhance the detection of NPs and NP-antibiotic complexes. The conical cavity structure of the substrate facilitates the enrichment and direct detection of NPs with diameters smaller than 450 nm. The three-dimensional (3D) F/M-AAO substrate achieved a limit of detection (LOD) of 1.73×10^6 ng/L for 100-nm NPs and a minimum detection concentration of 10^{-10} M for ciprofloxacin adsorbed on NPs (NPs-CIP). It demonstrated remarkable sensitivity and selectivity in the detection of both individual NPs and NP-antibiotic complexes. This work highlights the innovative application of the F/M-AAO substrate in the SERS detection of NPs and NP-antibiotic complexes, providing a low-cost and effective platform for monitoring emerging environmental contaminants.

Keywords: synergistic SERS enhancement, organic/MoS_2 composite, nanoplastics

PACS: 74.25.nd, 72.80.Tm, 88.20.rb

DOI: 10.1088/1674-1056/ada888 **CSTR:** 32038.14.CPB.ada888

1. Introduction

The growing crisis of nanoplastics (NPs) pollution poses a significant threat to global environmental health.[1] These particles, usually less than 1000 nm in diameter, are widespread in ecosystems and have been found in various biological organisms, including humans.[2] The positively charged surface of NPs enhance their adsorption of other contaminants, potentially increasing their ecological and health impacts. Their capacity to adsorb a range of environmental contaminants, including heavy metals,[3] organic pollutants and antibiotics,[4] ecological impact and health risks.[5,6] Despite research efforts, the detection of NPs remains a challenge. NPs, with dimensions typically below the resolution threshold of conventional optical microscopy, present a challenge for direct detection. The stable macromolecular cluster structure of NPs and the low concentrations of adsorption contaminants result in a small Raman scattering cross section, making them difficult to fit into traditional Raman detection.[7,8] These limitations have hindered a comprehensive understanding of the distribution, behavior, and ecological implications of NPs.[9,10]

Surface-enhanced Raman scattering (SERS) has become an important analytical tool due to its high sensitivity, molecular specificity, and non-destructive nature.[11,12] SERS, which is based on electromagnetic (EM) enhancement by modifying the shape, size, and type of noble metal, is ideal for the rapid and sensitive detection of NPs and associated contaminants.[13] Liu *et al.* and Chang *et al.*, have utilized V-shaped and nanotrap SiO_2@Ag SERS substrate to detect microplastic (MPs) and NPs, respectively.[14,15] Zhang *et al.* designed an array of gold triangular cavities and demonstrated effective SERS detection of polystyrene nanoplastics (PS-NPs).[16] However, current SERS substrates used for NP analysis are limited by their high cost,[17] dependence on single enhancement modes,[18] and lack of sensitivity and selectivity.[19]

Abdur Rahim *et al.* developed an novel three-dimensional (3D) SERS substrate fabricated with 2,3,5,6-tetrafluoro-tetracyanoquinodimethane (F_4TCNQ) and molybdenum disulfide (MoS_2) composites combined with anodic aluminum oxide (AAO) templates (F_4TCNQ/MoS_2/AAO, F/M-AAO) to achieve the detection of heavy metal ions (Hg^{2+}) in aqueous pollutants.[20] Although it is an innovation in non-metal SERS, the enhancement mechanism for the pollutants is ambiguous, and its applications are confined to the detection of soluble liquid pollutants. Actually, the V-shaped F/M-AAO substrate has broader applications in the SERS detection of

†Corresponding author. E-mail: liumei@sdnu.edu.cn

© 2025 Chinese Physical Society and IOP Publishing Ltd. All rights, including for text and data mining, AI training, and similar technologies, are reserved.

NPs. Its 3D structure not only achieves confinement of incident light within the cavity, but also enables the screening and enrichment of NPs with different sizes, effectively addressing the challenge of distinguishing between NPs and MPs. The organic/inorganic heterostructure provides EM enhancement for NPs and simultaneously provides chemical (CM) enhancement for other contaminants adsorbed on them. This approach allows us to explore the synergistic enhancement effects of the non-metallic hybrid SERS substrate on PS-NPs contamination and provides a reliable platform for highly sensitive and specific detection in environmental monitoring.

In this study, we investigated the SERS properties of PS-NPs and the combined contaminants of PS and ciprofloxacin (PS-CIP) using the 3D F/M-AAO substrate. The conical cavity structure of the 3D F/M-AAO substrate improved the limit of detection (LOD) for 100-nm PS-NPs to 1.73×10^{6} ng/L. In addition, the substrate achieved an ultra-high sensitivity LOD of 10^{-10} M for PS-CIP, demonstrating excellent stability and practicality. This study offers a straightforward and efficient means of analyzing NPs and their associated adsorbents, providing a robust platform for the sensitive and specific detection of emerging environmental contaminants using SERS.

2. Materials and methods

2.1. Preparation of F/M-AAO

The detailed procedure for the preparation of 3D F/M-AAO SERS substrates is described in detail in the literature.[20] For comparison, a reference sample was prepared using flat sapphire substrates (F/M-Al_2O_3). The fabrication and SERS testing of the F/M-AAO substrate is described in Fig. 1.

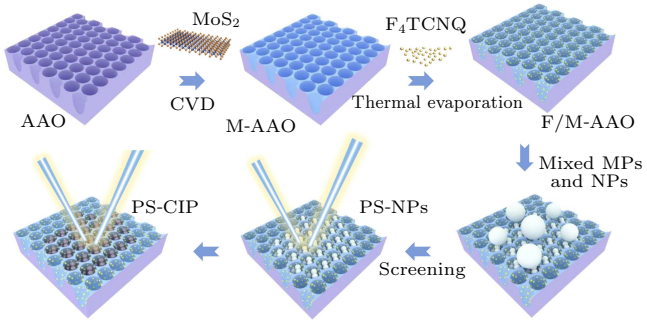


Fig. 1. Schematic illustration of the preparation and SERS process of the F/M-AAO substrate.

2.2. SERS measurements

The SERS properties of F/M-AAO was performed using Rhodamine 6G (R6G) as a basic probe. PS nanospheres, mixed micro and nanoplastic spheres, and PS-CIP were utilized as application probes. Aqueous solutions of R6G and PS at different concentrations were prepared by dilution. PS (1 mL, 100 nm in diameter), polyethylene terephthalate (PET) (1 mL, 3 μm in diameter), and polymethyl methacrylate (PMMA) particles (1 mL, 1.8 μm in diameter) were combined to form a mixed dispersion at a concentration of 1×10^{6} ng/L. The mixed solution was sonicated at 25 °C for 1 hour to ensure uniform distribution of the particles. Solutions of different concentrations were then dropped onto the F/M-AAO substrates and air dried at room temperature. For antibiotic adsorption detection, PS nanospheres were used as carriers following a standardized isothermal adsorption to ensure uniform mixing and complete antibiotic adsorption. A ciprofloxacin hydrochloride (CIP-HCl) stock solution was mixed with diluted PS nanosphere dispersion (1×10^{6} ng/L, 100 nm) to a final volume of 10 mL, with antibiotic concentrations logarithmically ranging from 10^{-11} M to 10^{-2} M. Triplicate samples were prepared for each concentration to ensure statistical validity. The mixtures were sonicated at 25 °C for 6 hours to ensure complete adsorption of the antibiotic on the PS nanospheres.

The enhancement factor (EF) and LOD of the SERS substrates were quantitatively evaluated using the formula reported in the literature.[21,22] For R6G, the EF and LOD were calculated using the 612-cm^{-1} peak, while for 100-nm PS, the 1003-cm^{-1} and 1032-cm^{-1} peaks were used. All values were derived by comparing powder samples under the same experimental conditions.

2.3. Sample characterizations

The surface morphology and elemental distribution of the samples were analyzed using a Zeiss Sigma 500 scanning electron microscopy (SEM) at accelerating voltages of 3 kV. The valence band (VB) or highest occupied molecular orbital (HOMO) of the sample can be obtained from ultraviolet photoelectron spectroscopy (UPS) measurements performed on a Thermo Scientific ESCALAB XI+ spectrometer using the He I line ($h\nu = 21.22$ eV) as the ultraviolet emission source. Ultraviolet–visible (UV-vis) absorption spectra were recorded using a Purkinje General TU-1900 spectrophotometer. The band gap of the sample can be determined from the photoluminescence (PL) spectra. Raman and PL spectra were characterized using a Horiba HR Evolution spectrometer. Raman measurements were performed using excitation wavelengths of 532 nm and 633 nm, while PL measurements were performed using an excitation wavelength of 325 nm. All tests were performed at room temperature to ensure consistency with standard environmental conditions.

3. Results and discussion

3.1. Properties of F/M-AAO

The F/M-AAO substrate exhibits distinct structures and properties that contribute to its enhanced SERS performance. The SEM image (Fig. 2(a)) reveals that F_4TCNQ nanoparticles, approximately 28 nm in diameter, uniformly cover the MoS_2 modified AAO (M-AAO) surface. The conical

pore structure of the AAO template concentrates MoS_2 and F_4TCNQ within the cavities. The E_{2g} and A_{1g} Raman peaks of MoS_2 at 385.5 cm^{-1} and 406.9 cm^{-1}, respectively, indicate the in-plane and out-of-plane vibrational modes (Fig. 2(b)). The frequency difference ($\Delta\nu$) of 23.4 cm^{-1} indicates the formation of a three-layer MoS_2 film in the F/M-AAO.[23] Compared to MoS_2 modified Al_2O_3 (M-Al_2O_3), the observed redshift of the E_{2g} and A_{1g} peaks of MoS_2 in the F/M-AAO composite suggests the compressive strain in the MoS_2 layers of the F/M-AAO composite.[24] This strain facilitates the deposition of F_4TCNQ organic molecules on the MoS_2 surface, leading to the formation of relatively isolated nanoislands. The peaks at 1105 cm^{-1}, 1245 cm^{-1}, 1397 cm^{-1}, 1451 cm^{-1}, and 1640 cm^{-1} in Fig. 2(c) are attributed to F_4TCNQ.[25] The Raman peak intensities of both F_4TCNQ and MoS_2 on the AAO substrate are significantly enhanced compared to those on the flat sapphire substrate. This enhancement is attributed to the large surface area provided by the distinctive inverted cone structure of the AAO template. It promotes the growth of numerous F_4TCNQ nanoparticles and provides a substantial interfacial area between the organic and inorganic phases, which is essential for efficient SERS activity.

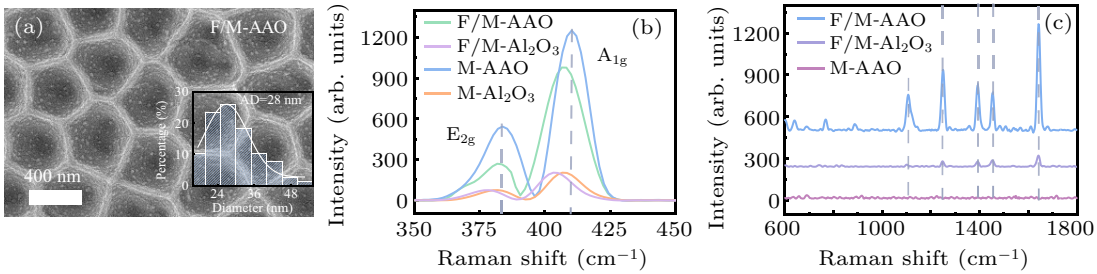


Fig. 2. Characterization of the fundamental properties of F/M-AAO. (a) SEM images of F/M-AAO. The inset shows the particle size distribution of F/M-AAO. (b) and (c) Raman spectra of different substrates in different ranges.

3.2. Basic SERS properties of F/M-AAO

R6G molecules were used to evaluate the fundamental SERS properties of the F/M-AAO composites. Figure 3(a) illustrates a comparison of the SERS activity of R6G molecules different substrates under 532-nm laser excitation. The Raman signal of R6G (10^{-7} M) was enhanced on the bare AAO substrate, but no signal was observed on the flat sapphire substrate. This indicates the conical structure of AAO contributes positively to SERS activity. The EF of M-AAO is approximately 3.45 times that of bare AAO. F/M-AAO exhibited the highest SERS activity with an EF of 23.2 times that of AAO. Figure 3(b) illustrates the linear correlation between Raman signal intensity and R6G concentration. The LOD for R6G was 3.67×10^{-14} M, with an EF of 1.82×10^{12} calculated from the SERS peak of a 10^{-15}-M R6G solution, demonstrating the high sensitivity of the SERS analysis. Figure 3(c) shows that R6G at 10^{-7} M exhibits SERS effects on the F/M-AAO substrate under both 532-nm and 633-nm laser excitations. R6G molecules display resonance Raman scattering (RRS) signals under 532-nm laser excitation, and their Raman signal is also significantly enhanced under 633-nm laser excitation due to the resonance excitation of the F/M-AAO substrate. Therefore, even if the probe molecules are not excited under optimal resonance conditions, the F/M-AAO substrate can still provide significant enhancement effects.

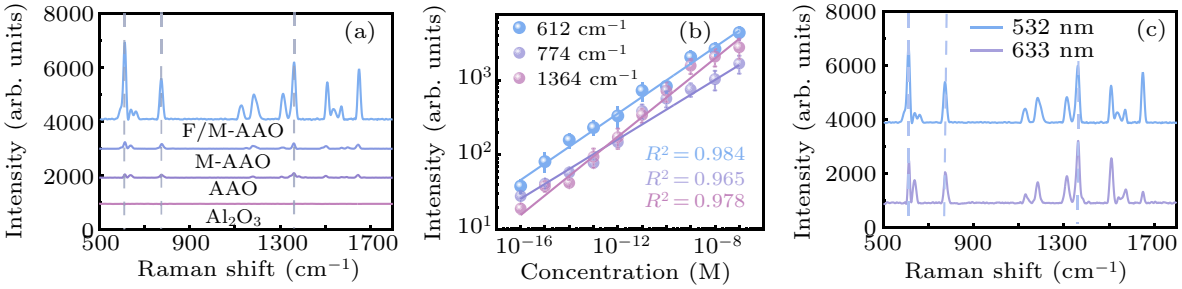


Fig. 3. SERS properties of R6G on F/M-AAO: (a) SERS results of R6G (10^{-7} M) on different substrates under a 532-nm laser, (b) the logarithmic relationship between SERS peak intensity and R6G concentration under 532-nm laser excitation, (c) SERS spectra of R6G (10^{-7} M) on F/M-AAO using different laser wavelengths.

3.3. SERS enhancement mechanisms of F/M-AAO

The SERS activity of the 3D F/M-AAO composite for R6G molecules is attributed to the synergistic effects of EM and CM enhancements. As shown in the UV-vis absorption spectra in Fig. 4(a), F/M-AAO substrate exhibits a significant absorption enhancement compared to the flat sapphire substrates. Compared to M-AAO, the absorption peaks of the F/M-AAO composites show redshifts with the strongest absorption peak positions corresponding to the energies of the 532-nm and 633-nm excitation lasers. This indicates that the

conical cavity structure of AAO enhances the light reflection and absorption within the cavity.[26]

Finite difference time domain (FDTD) solution simulations further elucidate the effect of the geometric configuration of the substrate on the electric field distribution. The simulations were based on the structural parameters of a typical substrate and referred to the literature.[20] Figure 4(b) shows that the electric fields of the incident laser and within the AAO cavity, denoted as $|E_0|$ and $|E|$, respectively. Under 532-nm and 633-nm laser excitations, the maximum ratio $|E|/|E_0|$ in the F/M-AAO cavity reaches 5.15 and 6.98, respectively. The significantly enhanced electric fields are formed near the organic F_4TCNQ nanoparticles and create localized "hot spots" that are uniformly distributed throughout the cavity. Simulations of the substrates excited by 532-nm and 633-nm lasers show similar patterns, confirming that the electromagnetic waves of the incident laser are multiply scattered by the conical cavity walls and absorbed by the MoS_2 layer and the F_4TCNQ nanoparticles, resulting in a light trapping phenomenon within the cavity. As a result, the absorption rate of incident light on the substrate surface was greatly enhanced, and the EM-SERS effect was generated on the probe molecules.

The CM-SERS activity of F/M-AAO is evidenced by the significant redshifts observed in the UV-vis spectra compared to M-AAO (Fig. 4(a)). This shift indicates a reduced energy gap in the composites, facilitated by the π-conjugated organic molecules, leading to an overlap of the electronic wave functions at the 2D inorganic/organic interface. The PL spectra in Fig. 4(c) reveal that the peak at 666 nm (peak A) can be fitted by the neutral exciton peak (X) and the negative exciton peaks (X^N) of MoS_2. The peak at 628 nm (peak B) corresponds to direct interband transitions of MoS_2. In F/M-AAO, the X peak displays a slight blueshift (0.07 nm) and increased intensity compared to M-AAO, while the B and X^N peaks show decreased intensity and a blueshift for the B peak (0.21 nm). This blueshift suggests a transition from charged negative to neutral excitons, indicating that charges have been transferred from the MoS_2 film into the F_4TCNQ nanoislands.[27]

The work function (ϕ) and the difference between the VB maximum and the Fermi energy level (E_{Fermi}), as determined by UPS, are 5.30 eV and 1.6 eV, respectively (Fig. 4(d)). The band gap of the F/M composite, determined by PL spectroscopy, is 1.87 eV. Based on these data, the electronic energy band structure and energy level diagram of the F/M-AAO can be constructed, as illustrated in Fig. 4(e). Charges are initially excited from the HOMO to the lowest unoccupied molecular orbital (LUMO) of F/M, and then transition to the LUMO of the adsorbed molecule (μ_{CT}). Raman photons are emitted when the charges return to the LUMO of F/M. Vibronic coupling facilitates charge transfer (CT) between the substrate and the molecule. In addition, the resonance-enhanced Raman scattering (RRS) of R6G (μ_{RRS-M}) can be achieved under 532-nm laser excitation. Under 633-nm laser excitation, the RRS of the F/M-AAO substrate enhances the excitation of charges to the LUMO of F/M (μ_{RRS-S}), improving the CT for the absorbed molecules. Thus, even if the molecules do not generate resonant Raman scattering under the incident laser, the RRS effect between the F/M-AAO composite and the incident laser can still induce SERS signals for the adsorbed molecules.

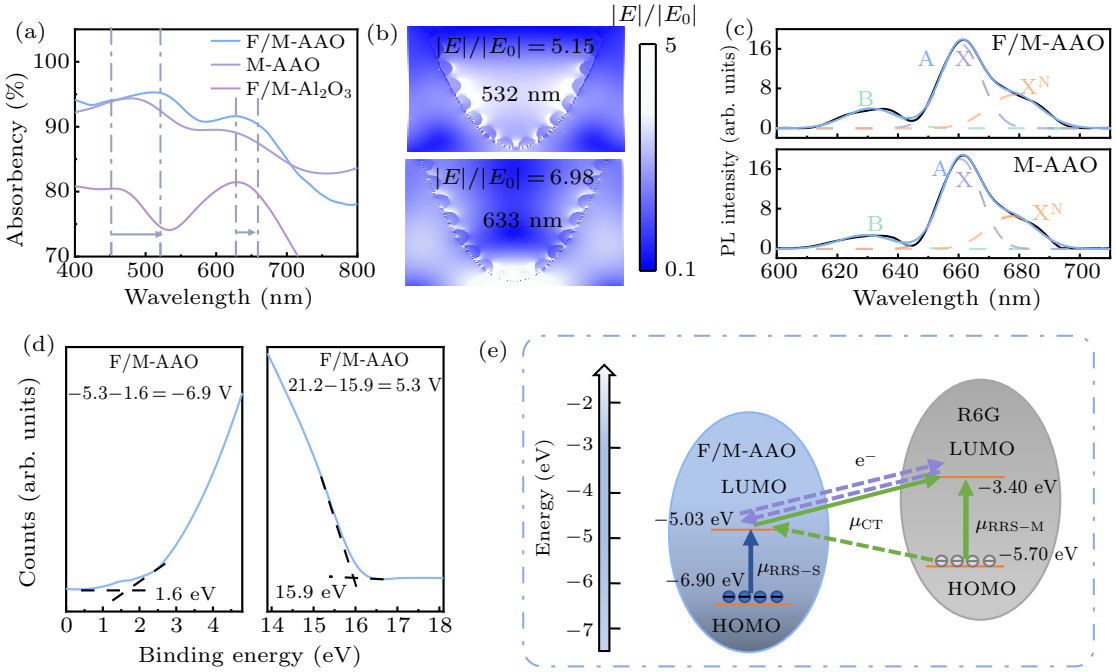


Fig. 4. The SERS enhancement mechanism of the F/M-AAO substrate: (a) UV-vis spectra of M-AAO, F/M-Al_2O_3, and F/M-AAO substrates; (b) near-field electric field distribution simulations of F/M-AAO composites under different excitation lasers; (c) PL spectra of M-AAO and F/M-AAO; (d) UPS spectra of F/M-AAO; (e) schematic representation of the CT mechanisms between F/M-AAO and R6G.

3.4. SERS performances of PS nanoparticles

We investigated the SERS detection of PS nanoparticles using the F/M-AAO composite. The F/M-AAO substrate has a unique conical cavity structure. The SEM image in Fig. 5(a) confirms the effective enrichment of PS nanoparticles within the conical pores of the F/M-AAO, with a uniform distribution of nanoparticles in each pore. The distinctive architecture ensures that nanoparticles of the optimal size are not only trapped but also retained within the cavity, enhancing their interaction with the laser excitation during SERS analysis. The corresponding FDTD simulation, shown in the inset of Fig. 5(a), illustrates that the PS nanospheres in the F/M-AAO cavities are surrounded by F_4TCNQ nanoislands closely adhering to the cavity walls. Although the PS-NPs do not exhibit resonance excitation under laser illumination, the electric field around the PS nanospheres is enhanced. This configuration optimizes the electromagnetic field effect and maximizes the Raman signal enhancement.

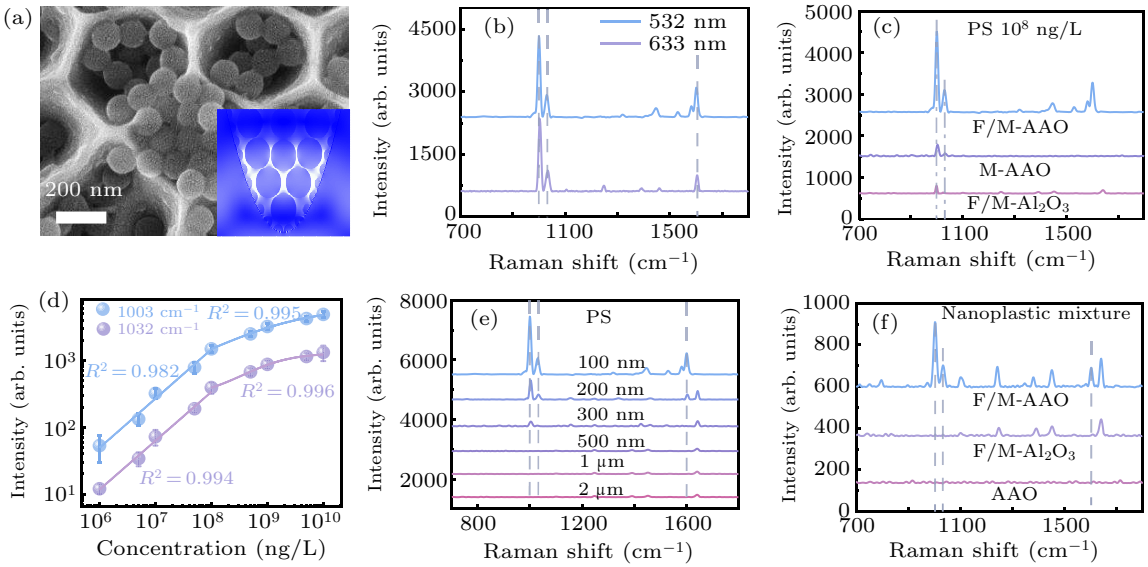


Fig. 5. SEM images and SERS properties of PS-NPs on F/M-AAO substrate: (a) SEM image of PS nanoparticles adsorbed on the F/M-AAO substrate. The inset shows the electric field distribution ($|E|/|E_0|$) around the F/M-AAO containing 100-nm PS nanoparticles. (b) Raman spectra of 100-nm PS nanoparticles (1×10^8 ng/L) on the F/M-AAO substrate, excited by different lasers. (c) Raman spectra of 100-nm PS nanoparticles (1×10^8 ng/L) on different substrates. (d) Relationship between SERS intensity and the concentration of PS-NPs. (e) Raman spectra of PS nanoparticles of different sizes (1×10^8 ng/L) on F/M-AAO substrate. (f) SERS results of mixed plastics on different substrates.

Table 1. Comparisons of acquired results with references for SERS detection of PS.

SERS substrate	Type of substrate	Nanostructure	Minimum size of PS (nm)	LOD (ng/L)	Reference
Au	metal	nanourchins	600	–	[28]
SiO_2PC@Ag	metal	nanowall	200	5×10^5	[15]
Au@Ag/AAO	metal	nanostars	400	5×10^8	[17]
Co_3O_4/Co_3S_4/Ag	semiconductor heterostructure	3D nanosheet arrays	100	1×10^8	[29]
D(C_7CO)-BTBT/MoS_2	semiconductor heterostructure	nanowall	100	4.5×10^5	[30]
F/M-AAO	semiconductor heterostructure	3D conical cavity arrays	100	1×10^6	this work

Figure 5(b) demonstrates the significant SERS activity of F/M-AAO for 100-nm PS nanoparticles at a concentration of 1×10^8 ng/L under 532-nm and 633-nm excitations. Under 532-nm excitation, the main characteristic peaks at 1003 cm^{-1} and 1032 cm^{-1} correspond to the ring breathing and C–H vibration of the benzene ring in PS nanoparticles. The Raman peak intensity at 1003 cm^{-1} for PS nanoparticles on the F/M-AAO substrate is approximately 13 times higher than that on the F/M-Al_2O_3 substrate (Fig. 5(c)). The EFs of PS nanoparticles absorbed on the F/M-AAO substrate at 1003 cm^{-1} and 1032 cm^{-1} were 9.43×10^3 and 5.74×10^3, respectively. The LOD for PS nanoparticles on F/M-AAO was as low as 1.73×10^6 ng/L (Fig. 5(d)), which is exceptionally sensitive for SERS analysis of PS nanoparticles as detailed in Table 1. In the concentration range of 10^6 ng/L to 10^8 ng/L, a linear relationship between the peak intensity and the concentration of PS nanoparticles is observed, with the coefficients of determination (R^2) of 0.982 and 0.994 for the 1003-cm^{-1} and 1032-cm^{-1} peaks, respectively.

It is noteworthy that when the concentration exceeds

1×10^8 ng/L, the accumulation of PS nanoparticles in the pores reaches saturation, which weakens the linear relationship, as illustrated in Fig. 5(d). The F/M-AAO nanostructure exhibits selectivity in the SERS detection of PS nanoparticles. PS nanoparticles smaller than 450 nm were successfully trapped within the cavities. Consequently, when the particle size exceeds 500 nm, the Raman signals are almost identical and relatively weak. When the particle size is smaller than the cavity diameter (450 nm), the SERS signal for 100-nm PS nanoparticles is enhanced by 1.6-fold and 4.7-fold compared to 200-nm and 300-nm PS nanoparticles at the same concentration, respectively (Fig. 5(e)). This enhancement is attributed to the size and number of nanoparticles that can fit into the cavity. Large nanoparticles are excluded from the cavity, resulting in weaker Raman signal enhancement. The SERS application of the F/M-AAO substrate was demonstrated by selectively detecting a mixture containing 100-nm PS nanoparticles, 1.8-μm PMMA and 3-μm PET particles. Figure 5(f) illustrates that the nanostructure of F/M-AAO effectively excludes the larger PMMA and PET particles from the nanocavities, allowing accurate identification and enhancement of Raman signals specific to the 100-nm PS nanoparticles.

3.5. SERS performances of PS-CIP

We utilized the SERS activity of F/M-AAO substrates to detect of PS-CIP contaminants. Antibiotic molecules are easily interfered by the fluorescence background under shorter wavelength laser excitation.[31] Therefore, we performed antibiotic detection under 633-nm laser excitation, as shown in Fig. 6(a). The SERS spectra of CIP-HCl are clearly discernible with minimal fluorescence interference. Under 633-nm laser illumination, the F/M-AAO substrate demonstrated a distinct advantage in the detection of CIP-HCl with Raman peaks at 745 cm^{-1}, 785 cm^{-1}, 1271 cm^{-1}, 1397 cm^{-1}, and 1630 cm^{-1}. The minimum detectable concentration of CIP by SERS is 1×10^{-8} M, which is close to the maximum residue limit (MRL) set by the European Union. The intensities of the Raman peaks at 1397 cm^{-1} and 1630 cm^{-1} correlated linearly with the concentration of the antibiotic, with R^2 values of 0.972 and 0.969, respectively.

Figures 6(d) and 6(e) display the SERS spectra of CIP-HCl adsorbed on PS nanoparticles at a fixed concentration of 10^6 ng/L for 100-nm NPs. Notably, the minimum detectable concentration of PS-CIP is as low as 10^{-10} M, which is two orders of magnitude more sensitive than that of CIP alone. In the concentration range of 10^{-2} M to 10^{-11} M, a logarithmic relationship is observed between the peak intensities at 1397 cm^{-1} and 1628 cm^{-1} and CIP concentration, with R^2 values of 0.990 and 0.997, respectively. At concentrations above 10^{-4} M, the SERS intensity of CIP adsorbed on PS nanoparticles is only slightly higher than that of pure CIP, probably due to the saturation of antibiotic adsorption on PS nanoparticles at high concentrations. These results highlight the potential of F/M-AAO substrates for sensitive and selective SERS detection of antibiotic contaminants in complex environmental samples.

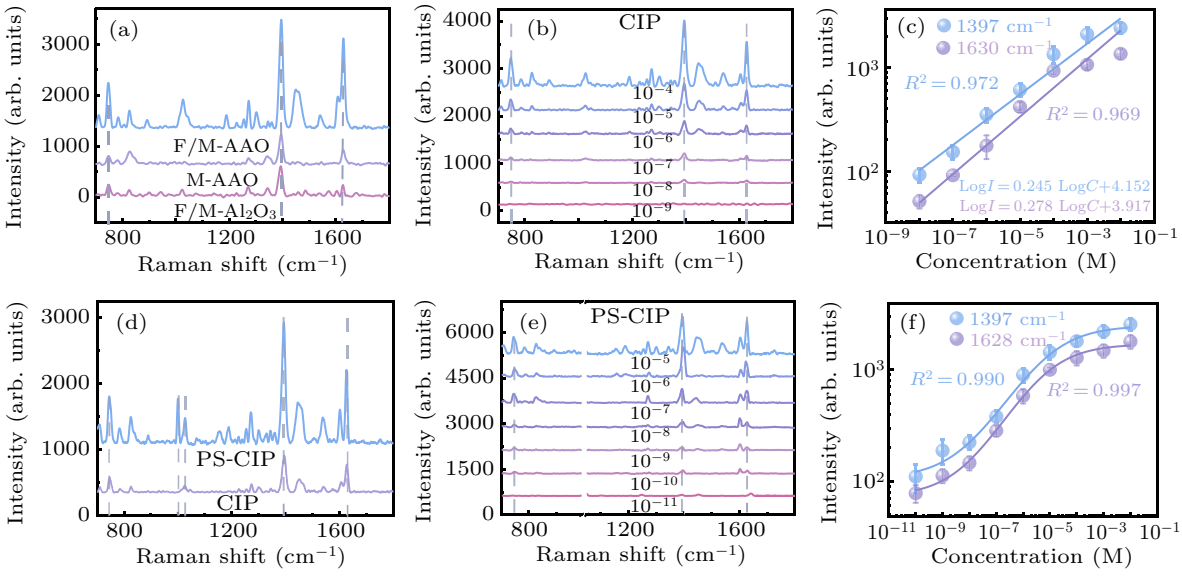


Fig. 6. SERS properties of CIP HCl and PS-CIP on F/M-AAO substrate: (a) SERS spectra of CIP on different substrates, (b) SERS spectra of CIP at different concentrations on F/M-AAO substrates, (c) logarithmic plot of SERS peak intensity versus CIP concentration, (d) SERS spectra of CIP and PS-CIP on F/M-AAO substrate, (e) SERS spectra of PS (1×10^6 ng/L, 100 nm in diameter) adsorbed with different concentrations of CIP, (f) logarithmic relationship between SERS intensity and PS-CIP concentration according to panel (e).

4. Conclusions

In this study, the highly sensitive SERS platform F/M-AAO, which integrates organic components with two-dimensional layered materials and a specific conical cavity structure, was successfully utilized to achieve the selective detection of NPs and demonstrate its effectiveness in the accurate detection of NPs, antibiotics, and the synergistic toxicity of PS-CIP contaminants. The platform enables the screening

and detection of NPs smaller than 450 nm with high sensitivity, achieving a detection limit of 1.73×10^6 ng/L when CIP is adsorbed on PS nanoparticles with a minimum detection concentration of 10^{-10} M. This work highlights the potential of F/M-AAO in detecting NPs contamination and improving the selectivity of NPs detection. These results represent a significant advancement in SERS technology, establishing F/M-AAO composites as a cost-effective, stable and effective platform for the detection of NPs, and represent a promising approach for the monitoring and specific detection of emerging environmental contaminants.

Acknowledgement

Project supported by the National Natural Science Foundation of China (Grant No. 12074229).

References

[1] Katare Y, Singh P, Sankhla M S, Singhal M, Jadhav E B, Parihar K, Nikalje B T, Trpathi A and Bhardwaj L 2022 *Biointerface Res. Appl. Chem.* **12** 3407
[2] Möller J N, Löder M G J and Laforsch C 2020 *Environ. Sci. Technol.* **54** 2078
[3] Luo H W, Liu C Y, He D Q, Xu J, Sun J Q, Li J and Pan X L 2022 *J. Hazard. Mater.* **423** 126915
[4] You X Q, Cao X Q, Zhang X, Guo J H and Sun W L 2021 *Environ. Int.* **157** 106842
[5] Carbery M, O'Connor W and Palanisami T 2018 *Environ. Int.* **115** 400
[6] Pirsaheb M, Hossini H and Makhdoumi P 2020 *Process Saf. Environ. Prot.* **142** 1
[7] Fang C, Sobhani Z, Zhang X, Gibson C T, Tang Y H and Naidu R 2020 *Water Res.* **183** 116046
[8] Caldwell J, Taladriz-Blanco P, Rothen-Rutishauser B and Petri-Fink A 2021 *Nanomaterials* **11** 1149
[9] Xie L F, Gong K D, Liu Y Y and Zhang L W 2023 *Environ. Sci. Technol.* **57** 25
[10] Yang T, Luo J L and Nowack B 2021 *Environ. Sci. Technol.* **55** 15873
[11] Jiang L, Hassan M M, Ali S, Li H H, Sheng R and Chen Q S 2021 *Trends Food Sci. Technol.* **112** 225
[12] Jiang S, Chang L, Luo J, Zhang J F, Liu X H, Lee C Y and Zhang W 2021 *Analyst* **146** 6170
[13] Liu J, Xu G J, Ruan X J, Li K J and Zhang L W 2022 *Front. Environ. Sci. Eng.* **16** 143
[14] Xu G J, Cheng H Y, Jones R B, Feng Y Q, Gong K D, Li K J, Fang X Z, Tahir M A, Valev V K and Zhang L W 2020 *Environ. Sci. Technol.* **54** 15594
[15] Chang L, Jiang S, Luo J, Zhang J F, Liu X H, Lee C Y and Zhang W 2022 *Environ. Sci.-Nano* **9** 542
[16] Zhang J J, Peng M, Lian E K, Xia L, Asimakopoulos A G, Luo S H and Wang L 2023 *Environ. Sci. Technol.* **57** 8365
[17] Le Q T, Ly N H, Kim M K, Lim S H, Son S J, Zoh K D and Joo S W 2021 *J. Hazard. Mater.* **402** 123499
[18] Li J, Liu H, Chen S Y, Liang X, Gao Y M, Zhao X F, Li Z, Zhang C, Lei F C and Yu J 2022 *J. Phys. Chem. Lett.* **13** 5815
[19] Silva A B, Bastos A S, Justino C I L, da Costa J A P, Duarte A C and Rocha-Santos T A P 2018 *Anal. Chim. Acta* **1017** 1
[20] Rahim A, Ma L Q, Saleem M, Lyu B, Shafi M, You Y X, Li M Y, Zhang X Y and Liu M 2024 *Adv. Sci.* **11** 2409838
[21] Wang G T, Wei H N, Tian Y, Wu M M, Sun Q Q, Peng Z S, Sun L F and Liu M 2020 *Opt. Express* **28** 18843
[22] Liu M, Hu X, Zhang C, Shafi M, Ma L, Lv B, Rahim A, Saleem M and Zhao L 2024 *Sens. Actuator B* **398** 134688
[23] Plechinger G, Heydrich S, Eroms J, Weiss D, Schüller C and Korn T 2012 *Appl. Phys. Lett.* **101** 101906
[24] Meilakhs A P and Koniakhin S V 2017 *Superlattices Microstruct.* **110** 319
[25] Xiao K, Rondinone A J, Puretzky A A, Ivanov I N, Retterer S T and Geohegan D B 2009 *Chem. Mater.* **21** 4275
[26] Zhang X, Suo H, Guo Y, Chen J K, Wang Y, Wei X H, Zheng W L, Li S H and Wang F 2024 *Nat. Commun.* **15** 6797
[27] Guan Y S, Qiao J, Liang Y Y, Bisoyi H K, Wang C, Xu W, Zhu D B and Li Q 2022 *Light-Sci. Appl.* **11** 236
[28] Lee C H and Fang J K H 2022 *J. Environ. Sci.* **121** 58
[29] Lv L L, He L, Jiang S Q, Chen J J, Zhou C X, Qu J H, Lu Y Q, Hong P Z, Sun S L and Li C Y 2020 *Sci. Total Environ.* **728** 138449
[30] Liu M, Zhang C, Ou C J, Hu X X, Saleem M, Rahim A, Ma L Q, Lv B J, Liu X H and Zhang W 2024 *Sens. Actuator B* **401** 135007
[31] Jiao A X, Cui Q Q, Li S, Li H S, Xu L L, Tian Y, Ma H, Zhang M Y, Liu X D and Chen M 2022 *Sens. Actuator B* **350** 130848